Microwave Magnetics

Sputtering Growth of Low-Damping Yttrium-Iron-Garnet Thin Films

Jinjun Ding [ID], Tao Liu, Houchen Chang [ID], and Mingzhong Wu

Department of Physics, Colorado State University, Fort Collins, CO 80523, USA

Abstract—This letter reports the development of low-damping yttrium-iron-garnet (YIG) thin films via sputtering. The films were deposited by sputtering at room temperature first and were then annealed in O_2 at high temperature. It is found that the annealing temperature critically affects the structural properties of the YIG films and thereby dictates the static and dynamic properties of the films. A 75 nm thick YIG film annealed at 900 °C shows an rms surface roughness of 0.08 nm, a coercivity of only 14 A/m (or 0.18 Oe), a saturation induction of 0.1778 T (or 1778 G), which is very close to the bulk value, a gyromagnetic ratio of 2.82×10^4 MHz/T (or 2.82 MHz/Oe), which almost matches the standard value, and a Gilbert damping constant of $\alpha \approx 5.2 \times 10^{-5}$, which is the lowest among the values reported so far for magnetic films in the nanometer thickness range. Frequency-dependent ferromagnetic resonance measurements with different field orientations confirmed that two-magnon scattering, if present, is very weak, and the measured damping value represents the actual damping of the YIG film.

Index Terms—Microwave magnetics, yttrium iron garnet, magnetic thin films, ferromagnetic resonance, Gilbert damping, sputtering, annealing temperature.

I. INTRODUCTION

Magnetic damping in yttrium iron garnet (**YIG**) $Y_3Fe_5O_{12}$ is lower than in any other magnetic materials. As such, YIG materials have been widely used in microwave devices, including phase shifters, isolators, and circulators [Pardavi-Horvath 2000, Harris 2009]. Recent years witnessed a strong interest in the use of YIG materials for spintronic and magnonic device applications. This interest derives mostly from the facts that the damping in YIG materials is two or three orders of magnitude lower than in ferromagnetic metals, and YIG-based devices may therefore enable faster domain wall motion, magnetization switching with lower currents, and more energy efficient information transfer than metal-based devices. In fact, there have been recent experimental demonstrations of spin-torque nano-oscillators [Arkook 2019] and logic gates [Goto 2019] that take advantage of nanometer-thick YIG films.

Spintronic and magnonic applications require YIG thin films with a thickness in the nanometer range, but it is challenging to grow YIG films that are nanometer thick but yet exhibit a damping comparable to the bulk value. There have been rather significant efforts in using liquid phase epitaxy (**LPE**), pulsed laser deposition (**PLD**), and magnetron sputtering methods to grow nanometer-thick YIG films [Heinrich 2011, Sun 2012, d'Allivy 2013, Chang 2014, Liu 2014, Lustikova 2014, Pirro 2014, Wang 2014, Howe 2015, Hauser 2016, Onbasli 2014, Tang 2016, Dubs 2017, Beaulieu 2018, Goto 2019, Yu 2019, Dubs 2020]. However, the Gilbert damping constants (α) of those films are still higher than the intrinsic damping in YIG single crystals, which is about 3×10^{-5} [Sparks 1964], and there is still room for the improvement of the damping of nanometer-thick YIG films. This letter reports the development of nanometer-thick YIG films via sputtering at room temperature and postannealing in O_2 at high temperature. The optimization of the annealing temperature enabled the realization of YIG films with $\alpha \approx 5.2 \times 10^{-5}$, which represents the lowest damping

Corresponding author: Mingzhong Wu (e-mail: mwu@colostate.edu).

J. Ding and T. Liu contributed equally to this work.

Table 1. Sputtering and annealing parameters for YIG film fabrication.

Sputtering			Annealing		
	Target-to-substrate distance	6.8 cm		Heating rate	10 °C/min
	Sample holder rotation rate	25 rpm		O_2 pressure	10 Torr
	Ar pressure	20 mTorr		Annealing temperature	800–1200 °C
	Ar flow	4 sccm		Annealing time	300 min
	Sputtering power	75 W		Cooling rate	2 °C/min
	Sputtering time	120 min			

reported so far for magnetic films, either metallic or insulating, thinner than 200 nm.

II. EXPERIMENTS

The YIG films were grown on single-crystal (111) $Gd_3Ga_5O_{12}$ (GGG) substrates by radio-frequency sputtering. The GGG substrate is rinsed sequentially with acetone, isopropyl alcohol, and deionized water, before being loaded into the sputtering chamber. A commercial YIG target with diameter of 2 in and a thickness of 0.25 in was used. The deposition is carried out at room temperature, at a rate of about 0.63 nm/min; prior to sputtering, the chamber system has a base pressure of 2.0×10^{-8} torr. The deposited YIG film is then annealed at high temperature in a separate chamber. The major sputtering and postannealing control parameters are summarized in Table 1. More details about the sputtering and annealing processes can be found in Chang [2014] and Liu [2014].

For the YIG films presented in this letter, the surface morphological properties were analyzed through tapping-mode atomic force microscopy (**AFM**) measurements. The crystalline structure and film thickness were characterized through X-ray diffraction (**XRD**) and X-ray reflectivity measurements, respectively. The static magnetic properties of the YIG films were measured by a vibrating sample magnetometer (**VSM**). The dynamic properties of the films were determined through ferromagnetic resonance (**FMR**) using X-band and K_u-band shorted rectangular waveguides and lock-in detection techniques. Shorted waveguide-based FMR approaches generally have lower signal-to-noise ratios and require the use of larger samples than microwave cavity-based FMR techniques, but they allow for measurements over a frequency range, in contrast to single-frequency measurements in the cavity FMR case. For the data presented below, the FMR frequency ranges from 8 to 17 GHz, and the sample size is
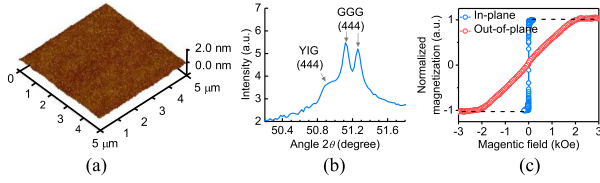
Fig. 1. AFM surface image, XRD spectrum, and magnetization versus field responses of a 75 nm YIG film. (a) AFM image. (b) XRD spectrum. (c) Magnetic hysteresis responses.
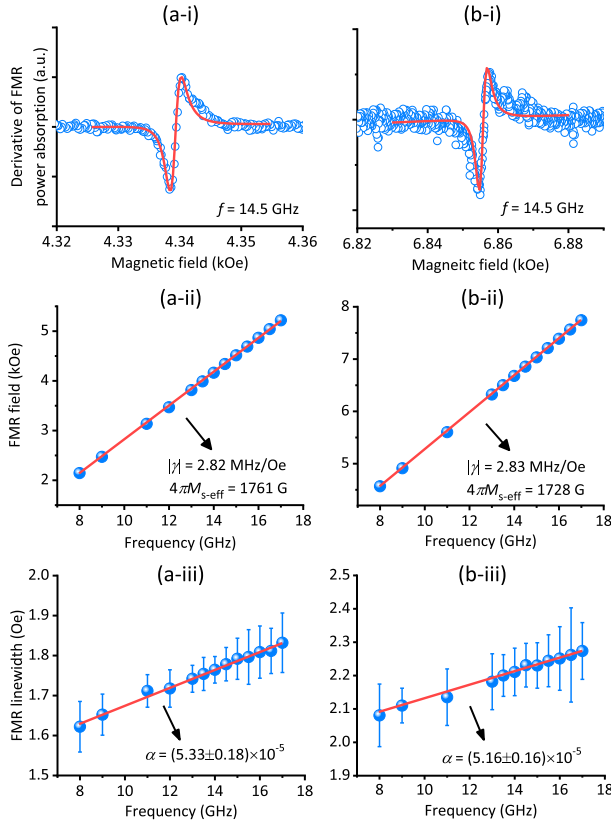

Fig. 2. FMR data on a 75 nm thick YIG film. The left and right columns show the data for (a) field IP and (b) OOP FMR measurements, respectively. In each column, the first graph shows an FMR profile and a Lorentzian fit. The second and third graphs show the FMR field and linewidth data, respectively, which were obtained via the Lorentzian fitting. In all the graphs, the blue symbols show the data, whereas the red lines show the fits.

about 1.5 by 1.5 mm. The analyses of the FMR data yielded the FMR field (H_{FMR}) and linewidth (ΔH) values of the films. Note that all the ΔH values presented below refer to the peak-to-peak linewidths of the FMR power absorption derivative profiles.

III. RESULTS AND DISCUSSIONS

For the data presented below, the YIG films are all 75 nm thick. They were prepared under the same conditions except that they were annealed at different temperatures. This section first presents and discusses the properties of the YIG film that shows the lowest damping among the films studied in this work. After that, the effects of the annealing temperature on the film structural, static magnetic, and damping properties are discussed in detail.

Figs. 1 and 2 show the representative data obtained for the YIG film that was annealed at 900 °C and shows the lowest damping.

Fig. 1(a) gives an AFM image that clearly indicates that the film has a very smooth surface; the analysis of the AFM data indicates a root-mean-square roughness of 0.08 ± 0.02 nm. Such smoothness allows for the fabrication of YIG-based bilayered structures with sharp interfaces for spintronic and magnonic device applications. Note that the surface roughness values in this work were all determined by averaging over AFM measurements on five different 5 μm × 5 μm areas on the film while the uncertainty for each roughness value is the corresponding standard deviation.

Fig. 1(b) shows an XRD spectrum that indicates the (111) orientation of the YIG film. This is expected because, first, the GGG substrate is (111) oriented and, second, the YIG lattice almost perfectly matches the GGG lattice [Sun 2013, Wang 2014]. Note that the lattice constants of YIG and GGG materials are 12.376 and 12.382 Å, respectively, at room temperature [Sun 2013]. Three important points should be made about the XRD spectrum. First, in Fig. 1(b), the YIG (444) peak appears as a relatively small hump on the left shoulder of the GGG (444) peak, and this hump can be much better resolved for other samples [see Fig. 3(a) and (b)]. Second, theoretically speaking, the YIG (444) peak should be present on the right side of the GGG (444) peaks according to Bragg's law, and the presence of the YIG (444) peak on the left side suggests that the YIG lattice has been expanded or enlarged vertically. The location of the YIG (444) peak on the opposite side of the GGG (444) peak has been previously reported [d'Allivy 2013, Howe 2015, Hauser 2016]. Possible reasons include: 1) lattice mismatching between the film and the substrate [Wang 2014, Fu 2017, Guo 2019, Li 2019] and 2) small off-stoichiometry, such as oxygen deficiency, in the film [Howe 2015]. For the YIG films in this work, it is believed that 2) is dominant over 1), because the YIG and GGG lattice constants are very close to each other, and the YIG films are also relatively thick and are therefore expected to be insensitive to the interfacial lattice mismatching. Third, the aforementioned lattice expansion may induce magnetoelastic anisotropy in the YIG film. For the films in this work, one can expect easy-plane anisotropy, as discussed in detail in Ding [2020]. This corresponds to $H_a < 0$, if one defines H_a as the effective field of the uniaxial perpendicular anisotropy in the film.

Fig. 1(c) presents magnetization versus field (H) hysteresis responses measured with a VSM system at different field directions, as indicated. The analysis of the data measured with an in-plane (**IP**) field yields a saturation induction ($4\pi M_s$) of about 1778 ± 15 G, which is very close to the bulk value (1750 G) [Sparks 1964], and a coercivity of about 0.18 Oe only, which indicates the presence of weak anisotropy and very few defects in the film. These VSM results, together with the AFM and XRD results, clearly suggest that the film is of high quality and is therefore expected to show low damping. The damping properties are presented below.

The top row in Fig. 2 shows the FMR data measured with an IP field. The blue circles in Fig. 2(a-i) show a representative FMR profile, which was measured at a frequency (f) of 14.5 GHz. The red curve shows a fit to a derivative Lorentzian trial function. Fig. 2(a-ii) and (a-iii) show H_{FMR} and ΔH, respectively, as a function of f. The dots show the experimental data obtained through the Lorentzian fitting, whereas the lines show numerical fits, which are explained below.

The line in Fig. 2(a-ii) is a fit to the Kittel equation

$$\omega = 2\pi \, |\gamma| \, \sqrt{H_{\mathrm{FMR}} \left(H_{\mathrm{FMR}} + 4\pi M_{s-\mathrm{eff}} \right)} \qquad (1)$$

where $\omega = 2\pi f$ is the angular frequency, $|\gamma|$ is the absolute gyromagnetic ratio, and $4\pi M_{s-\mathrm{eff}}$ denotes $4\pi M_s - H_a$. H_a is the effective field of a perpendicular anisotropy in the YIG film; "$H_a > 0$" and "$H_a < 0$" correspond to an easy-axis anisotropy along the film normal direction and an easy-plane anisotropy in the film plane, respectively. One physical origin of H_a is the above-discussed magnetoelastic anisotropy associated with the lattice expansion in the YIG film [Ding

2020]. The other is associated with the magnetocrystalline anisotropy in the YIG film. In brief, single-crystal YIG materials exhibit cubic magnetocrystalline anisotropy, with anisotropy constants $K_1 = -6100$ erg/cm^3 and $K_2 = -260$ erg/cm^3 [Sun 2013]. For a (111)-oriented YIG film, such a crystalline anisotropy gives rise to an easy-axis anisotropy along the film normal direction that can be described by an effective field

$$H_a = \frac{2\,|K_1|}{M_s} + \frac{4\,|K_2|}{M_s}. \tag{2}$$

Taking $4\pi M_s = 1778$ G presented earlier, one can use (2) to calculate and obtain $H_a \approx 94$ Oe. Note that the actual H_a associated with the magnetocrystalline anisotropy in the YIG film should be smaller than 94 Oe because the film is not single crystal. The linear fitting in Fig. 2(a-ii) yields $4\pi M_{s-\mathrm{eff}} = 1761$ G, which indicates an anisotropy field of $H_a = 4\pi M_s - 4\pi M_{s-\mathrm{eff}} \approx 17$ Oe. A discussion about this H_a value is presented shortly. The fitting also yields $|\gamma| = 2.82$ MHz/Oe, which is very close to the standard value (2.8 MHz/Oe).

The line in Fig. 2(a-iii) is a numerical fit to

$$\Delta H = \frac{2\alpha}{\sqrt{3}\,|\gamma|}\,\frac{\omega}{2\pi} + \Delta H_0 \tag{3}$$

where ΔH_0 denotes the line broadening due to the spatial inhomogeneity in the YIG film. The fitting gives $\alpha = (5.33 \pm 0.18) \times 10^{-5}$ and $\Delta H_0 = 1.46 \pm 0.06$ Oe, which are key results of this work, as discussed shortly. It should be noted that the damping constant and its error were obtained through the mathematical least-square fitting of the mean values of ΔH excluding their error bars. The purpose of presenting the error bars of the ΔH data points in Fig. 2(a-iii) is to show the quality of the Lorentzian fitting of the FMR profiles, such as the fitting shown in Fig. 2(a-i).

It is known that if present, two-magnon scattering can contribute to ΔH and thereby changes the slope of the ΔH versus f response, making it bigger or smaller, or turn an otherwise linear response to a curve response [McMichael 2004, Krivosika 2007, Kalarickal 2008, Lu 2012]. As such, the aforementioned α value may not represent the true damping in the film. To check this, FMR measurements were also carried out in an out-of-plane (**OOP**) field configuration in which there is no degenerate spin-wave modes at the FMR frequency and two-magnon scattering is therefore prohibited. The bottom row of Fig. 2 shows the data. The graphs are shown in the same format as those in the left column, to ease the comparison. The line in Fig. 2(b-ii) is a fit to

$$\omega = 2\pi\,|\gamma|\,(H_{\mathrm{FMR}} - 4\pi M_{s-\mathrm{eff}}) \tag{4}$$

whereas the line in Fig. 2(b-iii) is a fit to (3). The linear fitting in Fig. 2(b-iii) yields $\alpha = (5.16 \pm 0.16) \times 10^{-5}$ and $\Delta H_0 = 1.92 \pm 0.07$ Oe. This damping value is only about 3.2% smaller than the value from the IP FMR measurements. This nearly perfect agreement clearly confirms that the two-magnon scattering, if present, is very weak in the YIG film.

The fitting in Fig. 2(b-ii) yields $4\pi M_{s-\mathrm{eff}} = 1728$ G, which indicates an anisotropy field of $H_a = 4\pi M_s - 4\pi M_{s-\mathrm{eff}} \approx 50$ Oe. Thus, one can see the two H_a values (17 and 50 Oe) from the FMR measurements are both positive and are both smaller than the value (94 Oe) expected according to (2). This result indicates that in the YIG film concerned here, the magnetocrystalline anisotropy ($H_a > 0$) is stronger than the magnetoelastic anisotropy ($H_a < 0$). Furthermore, one can see that the H_a values from the IP and OOP FMR measurements do not match with each other. Possible reasons for this mismatching include

Table 2. Properties of YIG thin films reported previously.

t (nm)	$4\pi M_s$ (G)	FMR field	$\alpha\,(\times10^{-5})$	ΔH (Oe) (FMR f)	ΔH_0 (Oe)	Reference
19	1670	In-plane	23	4.0 (15 GHz)	2.9	Sun [2012]
20	1700	In-plane	23	3.5 (15 GHz)	2.1	d'Allivy [2013]
22.3	1795	Out-of-plane	8.6	6.9 (15 GHz)	6.4	Chang [2014]
23	1600	In-plane	18	2.4 (15 GHz)	1.2	Howe [2015]
56	1795	In-plane	6.2	1.4 (12 GHz)	1.1	Hauser [2016]
79	1721	In-plane	22	2.5 (14 GHz)	1.5	Onbasli [2014]
106	1780	Out-of-plane	12	1.2 (14 GHz)	0.4	Dubs [2017]
42	1724	Out-of-plane	9	1.8 (15 GHz)	1.5	Dubs [2020]
75	1778	Out-of-plane	5.2	2.2 (15 GHz)	1.9	This work

misalignment of the magnetic field during the FMR measurements and errors in the field measurements.

The aforementioned α values represent the lowest value reported so far for magnetic films, either metallic or insulating, thinner than 200 nm. This low damping is associated with the high structural quality of the YIG film that is evidently indicated by the very small surface roughness, very small H_c, and similarity of both $4\pi M_s$ and $|\gamma|$ to the standard values. In general, the damping in magnetic insulators may consist of an intrinsic contribution from magnon-phonon scattering and an extrinsic contribution from two-magnon scattering [Sparks 1964]. In the YIG film concerned here, the two-magnon scattering process is very weak, as indicated by the linear behavior of the ΔH versus f response over the entire 8–17 GHz range shown in Fig. 2(a-iii) and the consistency of the IP and OOP FMR measurements shown in Fig. 2(a-iii) and (b-iii). This result is most likely because the density of the defects in the film is low. The very smooth surface suggests the absence of large imperfections on the film surface, whereas the very small coercivity and the consistency of $4\pi M_s$ with the bulk value indicate the absence of high-density defects in the film bulk.

Table 2 compares the properties of the YIG film discussed earlier with those of some YIG films reported previously. One can see that the films showing relatively small damping values all exhibit a $4\pi M_s$ value relatively close to the bulk value. It should be noted that Table 2 serves to provide an overview of the properties of YIG thin films in recent studies, and a rigorous comparison of the listed α values may be inappropriate because the actual α values also depend on, first, the FMR measurement techniques and, second, the data analysis approaches, in particular, when multiple peaks appear in the FMR profiles.

In addition to the damping constant α, ΔH is also a relevant parameter for certain device applications. In addition, ΔH_0 is also a very useful parameter because it speaks about the spatial homogeneity of the films. In consideration of these facts, Table 3 compares α, ΔH, and ΔH_0 values, as well as the thickness and $4\pi M_s$ values, of several YIG thin films with $\alpha \leq 2.3 \times 10^{-4}$. The third column indicates the direction of the static magnetic field relative to the film plane during the FMR measurements. The fifth column lists ΔH values measured at or near 15 GHz. All ΔH and ΔH_0 values are peak-to-peak linewidths.

One can see from the data in Table 3 that even though the YIG film in this work shows the lowest α value, its ΔH and ΔH_0 values are not the lowest. The 106 nm film, which was grown by the LPE method, has both the lowest ΔH and ΔH_0 values [Dubs 2017], among all the films. For the films thinner than 100 nm, the 56 nm YIG film, which was grown by the PLD technique, shows the lowest ΔH and ΔH_0 values [Hauser 2016]. The fact that these two films exhibit smaller ΔH and ΔH_0 values than the YIG film in this work may suggest that LPE and PLD are better techniques than sputtering in terms of the realization of nanometer-thick, highly homogeneous, low ΔH YIG films. It may also result from the use of different FMR measurement techniques.

Table 3. Static magnetic and FMR properties of nanometer-thick, low-damping YIG thin films reported previously.

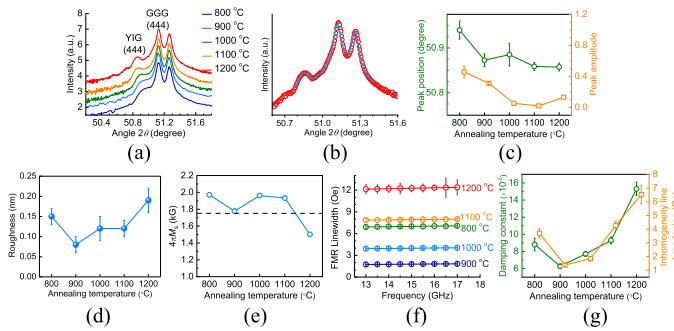| Thickness (nm)	$4\pi M_S$ (G)	FMR field Config.	α ($\times 10^{-5}$)	ΔH (Oe) (FMR frequency)	ΔH_0 (Oe)	Reference
19	1670	In-plane	23	4.0 (15 GHz)	2.9	[Sun 2012]
20	1700	In-plane	23	3.5 (15 GHz)	2.1	[d'Allivy 2013]
22.3	1795	Out-of-plane	8.6	6.9 (15 GHz)	6.4	[Chang 2014]
23	1600	In-plane	18	2.4 (15 GHz)	1.2	[Howe 2015]
56	1795	In-plane	6.2	1.4 (12 GHz)	1.1	[Hauser 2016]
79	1721	In-plane	22	2.5 (14 GHz)	1.5	[Onbasli 2014]
106	1780	Out-of-plane	12	1.2 (14 GHz)	0.4	[Dubs 2017]
42	1724	Out-of-plane	9	1.8 (15 GHz)	1.5	[Dubs 2020]
75	1778	Out-of-plane	5.2	2.2 (15 GHz)	1.9	This work

Fig. 3. Effects of the postannealing temperature on the properties of YIG thin films. (b) (Red circles) Experimental XRD data measured on the film annealed at 1200 °C. (Blue circles) Data in (c) were obtained from fitting, such as that shown in (b). Error bars in (c), (d), (f), (g) are standard deviation values from the numerical analyses or fitting (described in the text). (a) XRD spectra. (b) Fitting of XRD spectrum. (c) Position and amplitude of YIG (444) peak. (d) Surface roughness. (e) Saturation induction. (f) FMR linewidth. (g) Damping and inhomogeneity line broadening.

The measurements in Dubs [2017] and Hauser [2016] were carried out using a strip line and a coplanar waveguide, respectively, with the help of a vector network analyzer. Depending on the widths of the strip line and the coplanar waveguide signal line, these FMR techniques may allow for measurements of film samples with size much smaller than the YIG sample in this work; in general, ΔH_0 is larger in films with larger dimensions.

The aforementioned discussions indicate that the damping properties of a YIG film depend on the structural properties of the film. This result is further elucidated by the data in Fig. 3, which were obtained on five YIG film samples annealed at different temperatures. Fig. 3(a) gives the XRD spectra. Fig. 3(b) illustrates the numerical fitting of the XRD profile. The red circles show the same profile as the red one in Fig. 3(a), whereas the blue curve shows a fit that consists of three Voigt functions: one for the YIG (444) peak and the other two for the GGG (444) peaks. Such fitting was performed for all the five profiles shown in Fig. 3(a); the fitting-yielded results are presented in

Fig. 3(c), where the left and right axes show the position of the YIG (444) peak and the amplitude of the YIG (444) peak normalized by the amplitude of the dominant GGG (444) peak, respectively. Fig. 3(d) and (e) shows the surface roughness and $4\pi M_s$ as a function of the annealing temperature (T_a). Fig. 3(f) gives ΔH versus f responses for the five samples, which were measured with IP fields. The symbols show the data, whereas the lines show fits to (3). The fitting-yielded α and ΔH_0 values are presented in Fig. 3(g).

The data in Fig. 3 indicate four important results. First, T_a plays a crucial role in the structural properties of the YIG thin films. This is evident from the evolution of the YIG (444) peak with T_a, which is shown in Fig. 3(a) and (c), the change of the surface roughness with T_a, which is shown in Fig. 3(d), and the dependence of the film spatial inhomogeneity on T_a, which is indicated by the ΔH_0 data shown in Fig. 3(g). Second, there is a strong correlation between the T_a dependences of the roughness, $4\pi M_s$, α, and ΔH_0 data; the films with small α values show small roughness values, close-to-bulk-value $4\pi M_s$, and small ΔH_0, and vice versa. Third, among the five annealing temperatures, 900 °C appears to be the best in terms of the realization of a smooth, homogeneous, low-damping YIG film. These results together show that T_a critically affects the structural properties of the YIG films and thereby plays an essential role in the damping properties of the films.

Three final remarks are as follows: 1) Previous and ongoing efforts on YIG film growth utilize mainly LPE, PLD, and sputtering techniques, but sputtering is a much more industry-friendly approach. 2) In order to clarify the role of T_a, the thicknesses of the YIG films were kept the same in this work, which is 75 nm. To realize low-damping films that are much thinner or thicker, one may need to use an annealing temperature other than 900 °C. 3) The damping analyses in this work were based on the Gilbert model, which does not capture two-magnon scattering. As a result, if the two-magnon scattering is present, strictly speaking one cannot use (3) to fit the ΔH data measured under IP fields, even though it is appropriate to use it to fit the OOP ΔH data. In this work, however, (3) is approximately valid because the two-magnon scattering is very weak, which is indicated by the linear behavior of the ΔH versus f response and the agreement of α values from the IP and OOP FMR measurements.

There are several future works that are of great interest. First, FMR linewidth in YIG thin films represents a complex subject. In addition to magnon-phonon scattering and two-magnon scattering, there are also valence-exchange, slowly relaxing impurity, and rapidly relaxing impurity mechanisms that contribute to the FMR linewidth of YIG materials, in particular, at low temperature [Sparks 1964]. It would be very interesting to separate and quantize the contributions of different mechanisms to the overall FMR linewidth in the nanometer-thick YIG films through comprehensive frequency, temperature, and field angle-dependent FMR measurements. Such studies may enable further improvement in the damping of nanometer-thick YIG films. Second, the YIG films in this work exhibits magnetoelastic anisotropy, which is uniaxial (along the film normal), and magnetocrystalline anisotropy, which is three-fold in the film plane. Future study is very interesting that takes advantage of field angle-dependent FMR measurements to determine the anisotropy axes and constants in the films [Makino 1981]. Third, the YIG films in this work have weak anisotropy, but certain device applications, such as racetrack memory [Bhatti 2017, Vélez 2019], may require YIG films with perpendicular anisotropy [Soumah 2018, Ding 2020, Lin 2020]. Future work is of great interest that explores the growth of YIG thin films that have a damping comparable to that reported earlier but also exhibit perpendicular anisotropy and square hysteresis loops.

ACKNOWLEDGMENT

REFERENCES

Arkook B, Safranski C, Rodriguez R, Krivorotov I N, Schneider T, Lenz K, Lindner J, Chang H, Wu M, Tserkovnyak Y, Barsukov I (2019), "Thermally driven two-magnet nano-oscillator with large spin-charge conversion," *arXiv:1909.12445*.

Beaulieu N, Kervarec N, Thiery N, Klein O, Naletov V, Hurdequint H, de Loubens G, Youssef J B, Vukadinovic N (2018), "Temperature dependence of magnetic properties of a ultrathin yttrium-iron garnet film grown by liquid phase epitaxy: Effect of a Pt overlayer," *IEEE Magn. Lett.*, vol. 9, 3706005, doi: 10.1109/lmag.2018.2868700.

Bhatti S, Sbiaa R, Hirohata A, Ohno H, Fukami S, Piramanayagam S N (2017), "Spintronics based random access memory: A review," *Mater. Today*, vol. 20, pp. 530–548, doi: 10.1016/j.mattod.2017.07.007.

Chang H, Li P, Zhang W, Liu T, Hoffmann A, Deng L, Wu M (2014), "Nanometer-thick yttrium iron garnet films with extremely low damping," *IEEE Magn. Lett.*, vol. 5, 6700104, doi: 10.1109/LMAG.2014.2350958.

d'Allivy Kelly O, Anane A., Bernard R, Ben Youssef J, Hahn C, Molpeceres A H, Carrétéro C, Jacquet E, Deranlot C, Bortolotti P, Lebourgois R, Mage J-C, de Loubens G, Klein O, Cros V, Fert A (2013), "Inverse spin Hall effect in nanometer-thick yttrium iron garnet/Pt system," *Appl. Phys. Lett.*, vol. 103, 082408, doi: 10.1063/1.4819157.

Ding J, Liu C, Zhang Y, Erugu U, Zhi Q, Yu R, McCollum E, Mo S, Yang S, Ding H, Xu X, Tang J, Yang X, Wu M (2020), "Nanometer-thick yttrium iron garnet films with perpendicular anisotropy and low damping," *Phys. Rev. Appl.*, submitted for publication.

Dubs C, Surzhenko O, Linke R, Danilewsky A, Brückner U, Dellith J (2017), "Submicrometer yttrium iron garnet LPE films with low ferromagnetic resonance losses," *J. Phys. D: Appl. Phys.*, vol. 50, 204005, doi: 10.1088/1361-6463/aa6b1c.

Dubs C, Surzhenko O, Thomas R, Osten J, Schneider T, Lenz K, Grenzer J, Hübner R, Wendler E (2020), "Low damping and microstructural perfection of sub-40nm-thin yttrium iron garnet films grown by liquid phase epitaxy," *Phys. Rev. Mater.*, vol. 4, 024416, doi: 10.1103/PhysRevMaterials.4.024416.

Fu J, Hua M, Wen X, Xue M, Ding S, Wang M, Yu P, Liu S, Han J, Wang C, Du H, Yang Y, Yang J (2017), "Epitaxial growth of $Y_3Fe_5O_{12}$ thin films with perpendicular magnetic anisotropy," *Appl. Phys. Lett.*, vol. 110, 202403, doi: 10.1063/1.4983783.

Goto T, Yoshimoto T, Iwamoto B, Shimada K, Ross C A, Sekiguchi K, Granovsky A B, Nakamura Y, Uchida H, Inoue M (2019), "Three port logic gate using forward volume spin wave interference in a thin yttrium iron garnet film," *Sci. Rep.*, vol. 9, 16472, doi: 10.1038/s41598-019-52889-w.

Guo C Y, Wan C H, Zhao M K, Wu H, Fang C, Yan Z R, Feng J F, Liu H F, Han X F (2019), "Spin-orbit torque switching in perpendicular $Y_3Fe_5O_{12}$/Pt bilayer," *Appl. Phys. Lett.*, vol. 114, 192409, doi: 10.1063/1.5098033.

Harris V G, Geilerab A, Chen Y, Yoon S D, Wu M, Yang A, Chen Z, He P, Parimi P V, Zuo X, Patton C E, Abe M, Acher O, Vittoriaab C (2009), "Recent advances in processing and applications of microwave ferrites," *J. Magn. Magn. Mater.*, vol. 321, pp. 2035–2047, doi: 10.1016/j.jmmm.2009.01.004.

Hauser C, Richter T, Homonnay N, Eisenschmidt C, Qaid M, Deniz H, Hesse D, Sawicki M, Ebbinghaus S G, Schmidt G (2016), "Yttrium iron garnet thin films with very low damping obtained by recrystallization of amorphous material," *Sci. Rep.*, vol. 6, 20827, doi: 10.1038/srep20827.

Heinrich B, Burrowes C, Montoya E, Kardasz B, Girt E, Song Y-Y, Sun Y, Wu M (2011), "Spin pumping at the magnetic insulator (YIG)/normal metal (Au) interfaces," *Phys. Rev. Lett.*, vol. 107, 066604, doi: 10.1103/PhysRevLett.107.066604.

Heyroth F, Hauser C, Trempler P, Geyer P, Syrowatka F, Dreyer R, Ebbinghaus S G, Woltersdorf G, Schmidt G (2019), "Monocrystalline freestanding three-dimensional yttrium-iron-garnet magnon nanoresonators," *Phys. Rev. Appl.*, vol. 12, 054031, doi: 10.1103/physrevapplied.12.054031.

Howe B M, Emori S, Jeon H-M, Oxholm T M, Jones J G, Mahalingam K, Zhuang Y, Sun N X, Brown G J (2015), "Pseudomorphic yttrium iron garnet thin films with low damping and inhomogeneous linewidth broadening," *IEEE Magn. Lett.*, vol. 6, 3500504, doi: 10.1109/LMAG.2015.2449260.

Kalarickal S S, Krivosik P, Das J, Kim K S, Patton C E (2008), "Microwave damping in polycrystalline Fe-Ti-N films: Physical mechanisms and correlations with composition and structure," *Phys. Rev. B*, vol. 77, 054427, doi: 10.1103/PhysRevB.77.054427.

Krivosika P, Mo N, Kalarickalb S, Patton C E (2007), "Hamiltonian formalism for two magnon scattering microwave relaxation: Theory and applications," *J. Appl. Phys.*, vol. 101, 083901, doi: 10.1063/1.2717084.

Li G, Bai H, Su J, Zhu Z Z, Zhang Y, Cai J W (2019), "Tunable perpendicular magnetic anisotropy in epitaxial $Y_3Fe_5O_{12}$ films," *APL Mater.*, vol 7, 041104, doi: 10.1063/1.5090292.

Lin Y, Jin L, Zhang H, Zhong Z, Yang Q, Rao Y, Li M (2020), "Bi-YIG ferrimagnetic insulator nanometer films with large perpendicular magnetic anisotropy and narrow ferromagnetic resonance linewidth," *J. Magn. Magn. Mater.*, vol. 496, 165886, doi: 10.1016/j.jmmm.2019.165886.

Liu T, Chang H, Vlaminck V, Sun Y, Kabatek M, Hoffmann A, Deng L, Wu M (2014), "Ferromagnetic resonance of sputtered yttrium iron garnet nanometer films," *J. Appl. Phys.*, vol. 115, 17A501, doi: 10.1063/1.4852135.

Lu L, Young J, Wu M, Mathieu C, Hadley M, Krivosik P, Mo N (2012), "Tuning of magnetization relaxation in ferromagnetic thin films through seed layers," *Appl. Phys. Lett.*, vol. 100, 022403, doi: 10.1063/1.3675614.

Lustikova J, Shiomi Y, Qiu Z, Kikkawa T, Iguchi R, Uchida K, Saitoh E (2014), "Spin current generation from sputtered $Y_3Fe_5O_{12}$ films," *J. Appl. Phys.*, vol. 116, 153902, doi: 10.1063/1.4898161.

Makino H, Hidaka Y (1981), "Determination of magnetic anisotropy constants for bubble garnet epitaxial films using field orientation dependence in ferromagnetic resonances," *Mater. Res. Bull.*, vol. 16, pp. 957–966, doi: 10.1016/0025-5408(81)90137-9.

McMichael R D, Krivosik P (2004), "Classical model of extrinsic ferromagnetic resonance linewidth in ultrathin films," *IEEE Trans. Magn.*, vol. 40, pp. 2–11, doi: 10.1109/TMAG.2003.821564.

Onbasli M C, Kehlberger A, Kim D H, Jakob G, Kläui M, Chumak A V, Hillebrands B, Ross C A (2014), "Pulsed laser deposition of epitaxial yttrium iron garnet films with low Gilbert damping and bulk-like magnetization," *APL Mater.*, vol. 2, 106102, doi: 10.1063/1.4896936.

Pardavi-Horvath M (2000), "Microwave applications of soft ferrites," *J. Magn. Magn. Mater.*, vol. 215/216, pp. 171–183, doi: 10.1016/S0304-8853(00)00106-2.

Pirro P, Brächer T, Chumak A V, Lägel B, Dubs C, Surzhenko O, Görnert P, Leven B, Hillebrands B (2014), "Spin-wave excitation and propagation in microstructured waveguides of yttrium iron garnet/Pt bilayers," *Appl. Phys. Lett.*, vol. 104, 012402, doi: 10.1063/1.4861343.

Soumah L, Beaulieu N, Qassym L, Carrétéro C, Jacquet E, Lebourgeois R, Youssef J B, Bortolotti P, Cros V, Anane A (2018), "Ultra-low damping insulating magnetic thin films get perpendicular," *Nature Commun.*, vol. 9, 3355, doi: 10.1038/s41467-018-05732-1.

Sparks M (1964), *Ferromagnetic-Relaxation Theory*. New York, NY, USA: McGraw-Hill.

Sun Y, Song Y-Y, Chang H, Kabatek M, Jantz M, Schneider W, Wu M, Schultheiss H, Hoffmann A (2012), "Growth and ferromagnetic resonance properties of nanometer-thick yttrium iron garnet films," *Appl. Phys. Lett.*, vol. 101, 152405, doi: 10.1063/1.4759039.

Sun Y, Wu M (2013), "Yttrium iron garnet nano films: Epitaxial growth, spin-pumping efficiency, and Pt-capping-caused damping," in *Solid State Physics*, vol. 64. Burlington, VT, USA: Academic, , pp. 157–191, doi: 10.1016/b978-0-12-408130-7.00006-x.

Tang C, Aldosary M, Jiang Z, Chang H, Madon B, Chan K, Wu M, Garay J E, Shi J (2016), "Exquisite growth control and magnetic properties of yttrium iron garnet thin films," *Appl. Phys. Lett.*, vol. 108, 102403, doi: 10.1063/1.4943210.

Vélez S, Schaab J, Wörnle M S, Müller M, Gradauskaite E, Welter P, Gutgsell C, Nistor C, Degen C L, Trassin M, Fiebig M, Gambardella P (2019), "High-speed domain wall racetracks in a magnetic insulator," *Nature Commun.*, vol. 10, 4750, doi: 10.1038/s41467-019-12676-7.

Wang H, Du C, Hammel P C, Yang F (2014), "Strain-tunable magnetocrystalline anisotropy in epitaxial $Y_3Fe_5O_{12}$ thin films," *Phys. Rev. B*, vol. 89, 134404, doi: 10.1103/PhysRevB.89.134404.

Wang H L, Du C H, Pu Y, Adur R, Hammel P C, Yang F Y (2014), "Scaling of spin Hall angle in 3d, 4d, and 5d metals from $Y_3Fe_5O_{12}$/metal spin pumping," *Phys. Rev. Lett.*, vol. 112, 197201, doi: 10.1103/PhysRevLett.112.197201.

Yu R, He K, Liu Q, Gan X, Miao B, Sun L, Du J, Cai H, Wu X, Wu M, Ding H (2019), "Nonvolatile electric-field control of ferromagnetic resonance and spin pumping in Pt/YIG at room temperature," *Adv. Electron. Mater.*, vol. 5, 1800663, doi: 10.1002/aelm.201800663.

Zhang D, Jin L, Zhang H, Yang Q, Rao Y, Wen Q, Zhou T, Liu C, Zhong Z, Xiao J Q (2017), "Chemical epitaxial growth of nm-thick yttrium iron garnet films with low gilbert damping," *J. Alloy Compd.*, vol. 695, pp. 2301–2305, doi: 10.1016/j.jallcom.2016.11.089.